ACS OMEGA

Article

http://pubs.acs.org/journal/acsodf

Serum Protein-Resistant Behavior of Multisite-Bound Poly(ethylene glycol) Chains on Iron Oxide Surfaces

Nicoletta Giamblanco,*,† Giovanni Marletta,*,† Alain Graillot,‡ Nicolas Bia,‡ Cédric Loubat,‡ and Jean-François Berret*,§

†Laboratory for Molecular Surface and Nanotechnology (LAMSUN), Department of Chemical Sciences, University of Catania and CSGI, Viale A. Doria 6, 95125 Catania, Italy

‡Specific Polymers, ZAC Via Domitia, 150 Avenue des Cocardières, 34160 Castries, France

§Matière et Systèmes Complexes, UMR 7057 CNRS, Université Denis Diderot Paris-VII, Bâtiment Condorcet, 10 rue Alice Domon et Léonie Duquet, 75205 Paris, France

Supporting Information

ABSTRACT: Recent surveys have shown that the number of nanoparticle-based formulations actually used at a clinical level is significantly lower than that expected a decade ago. One reason for this is that the physicochemical properties of nanoparticles fall short for handling the complexity of biological environments and preventing nonspecific protein adsorption. In this study, we address the issue of the interactions of plasma proteins with polymer-coated surfaces. With this aim, we use a noncovalent grafting-to method to functionalize iron oxide sub-10 nm nanoparticles and iron oxide flat substrates and compare their protein responses. The functionalized copolymers consist of alternating poly(ethylene glycol) (PEG) chains and phosphonic acid grafted on the same backbone. Quartz crystal microbalance with dissipation was used to monitor polymer adsorption kinetics and evaluate the resistance to protein adsorption. On flat substrates, functionalized PEG copolymers adsorb and form a brush in moderate or highly stretched regimes, with densities between 0.15 and 1.5 nm^{-2}. PEG layers using phosphonic acid as linkers exhibit excellent protein resistance. In contrast, layers prepared with carboxylic acid as the grafting agent exhibit mitigated protein responses and layer destructuration. The present study establishes a correlation between the long-term stability of PEG-coated particles in biofluids and the protein resistance of surfaces coated with the same polymers.

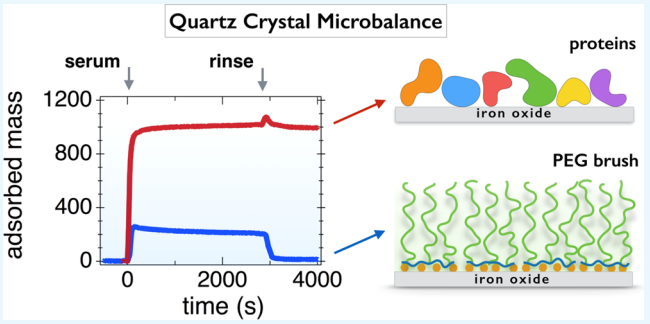

I. INTRODUCTION

In nanomedicine, the possibility of using engineered nanoparticles for medical imaging and therapy has attracted much interest over the last 15 years. Recent surveys have shown, however, that nanotechnology-based formulations have not been as successful as initially thought.[1] The number of nanoparticle carriers actually used to improve patient outcomes at a clinical level is significantly lower than that expected a decade ago. Today, most therapeutic drug-carrying particles are in the form of liposomes, lipid-based complexes, or biodegradable polymer/drug combinations. More complex nanoformulations, including inorganic particles, have been barely exploited or are still in clinical trials. One of the reasons for these mixed results is related to the difficulty in matching the physicochemical properties of nanoparticle carriers to the constraints of biological environments and, in particular, in preventing ubiquitous nonspecific protein adsorption. For a vast majority of nanoformulations, particles administered in vivo are recognized by plasma proteins and eliminated from the blood stream within a few minutes, leading to their accumulation in unrelated organs, such as the liver and kidneys.[2,3]

On the physicochemical side, it is now well established that for biological applications nanoparticle surfaces need to be modified to prevent protein adsorption. A great deal of surface functionalization methods have been developed and assessed either in vitro or in vivo. The most advanced strategies have been based on modified or grafted polymers,[4−11] although new fabrication techniques using supported bilayer or biomembrane mimetics are currently being evaluated.[12] In polymers, surface functionalization is achieved either by physical adsorption methods (such as spin-coating, layer-by-layer assembly, and solvent-casting)[13,14] or chemical bonding methods based on surface-initiated polymerization[10,11] or surface activation by means of radiation treatments.[15−17] Surface functionalization takes advantage of the extended library of polymer architectures (linear chains, copolymers, stars, and dendrimers) and chelating agents that were developed in polymer and coordination chemistry.[18−24] Hydrosoluble neutral polymers, such as poly-

Received: January 4, 2017
Accepted: February 28, 2017
Published: April 5, 2017

DOI: 10.1021/acsomega.7b00007
ACS Omega 2017, 2, 1309−1320

(ethylene glycol) (PEG), polyacrylamide, and some polysaccharides, show improved protein resistance (as compared to that of ion-containing chains) and have been incorporated into nanomedicine formulation synthesis. Among the polymers tested, PEG is the most studied bioresistant polymer.[3,21,23−33] Apart from being inexpensive and approved by regulatory and control agencies, PEG offers many advantages. Made of a sequence of $-CH_2-CH_2-O-$ monomers, PEG is a flexible macromolecule and can be synthesized with a narrow molecular weight dispersity. Moreover, PEG was also found to accurately follow polymer dynamics predictions,[34,35] so it allows quantitative evaluation of the chain conformation, in view of the importance of this factor in determining the adsorption protein behavior.

For polymers at curved or flat interfaces, chain conformations may be strikingly different. Alexander and de Gennes were the first to describe theoretically the conformational behavior of polymers at interfaces and, specifically, polymers tethered by one extremity and having the remaining part of the chain dangling in the solvent.[36,37] For flat surfaces, two main regimes were predicted.[37,38] At low polymer densities, that is, $\sigma < 1/\pi R_g^2$, where R_g is the gyration radius of the chains under good solvent conditions, the polymers adopt a so-called mushroom configuration. In this first case, the adlayer thickness is twice the gyration radius. At higher densities, that is, $\sigma > 1/\pi R_g^2$, monomer−monomer excluded volume interactions induce stretching of the chains, which then enter the brush regime. In this configuration, the height increases and varies as $h \sim \sigma^{\nu} N$, where N is the degree of polymerization and ν, a coefficient between 1/3 and 1 that depends on solvent quality.[38−40] It is commonly admitted that the soft interfaces represented by hydrosoluble polymer brushes are excellent protein repellents.[6,15,21,25,27,30,41−43] Polymer adlayers or brushes are generally regarded as steric repulsive barriers. Recent studies have shown, however, that protein interactions with soft interfaces are far more complex and that the brushes act as kinetic barriers rather than efficiently preventing adsorption.[42]

The present report aims at establishing a correlation between the stability of PEGylated particles in biological environments and the protein resistance of PEGylated surfaces coated with the same polymers. To this end, we used a noncovalent grafting-to method to deposit functionalized PEG copolymers on iron oxide substrates under environmentally friendly conditions, that is, in aqueous media and at room temperature. The copolymers studied consist of alternating PEG chains (of molecular weight 1000, 2000, and 5000 g mol^{-1}) and acidic moieties grafted on the same backbone. The deposition on iron oxide is driven by the acid groups, which are of two kinds, carboxylic acid and phosphonic acid. Phosphonic acid is known to have a higher affinity toward metals or metal oxides compared to that of sulfates and carboxylates, and it is anticipated that these residues will build stronger links with the surface.[21−23,32,41,44,45] This research follows up recent pharmacokinetics studies showing that sub-10 nm iron oxide nanoparticles coated with the above polymers circulate in the blood pool for over 2 h without being recognized by the mononuclear phagocytic system.[24] The circulation time was about 50 times higher than that of non-PEGylated probes and benchmarks, a feature that was unequivocally attributed to the coating. To study the interaction of PEGylated polymers and proteins with iron oxide substrates, quartz crystal microbalance with dissipation (QCM-D) was carried out with a twofold objective: (i) to monitor the polymer adsorption kinetics and derive the adlayer structure and (ii) to evaluate the protein resistance of the built-up layers. By varying parameters such as the acid−base conditions, polymer molecular weight, and nature of the grafting agent, different protein resistance performances were obtained, with values ranging typically from 65 to 99% of repulsion efficacy. Interestingly, we have found a positive correlation between the strength of the PEG−substrate linkage, the stability of PEGylated nanoparticles, and the protein resistance determined by QCM-D.

II. EXPERIMENTAL SECTION

II.I. Polymer Synthesis and Characterization. *II.I.I. Synthesis.* Poly(ethylene glycol methacrylate-*co*-dimethyl-(methacryoyloxy) methyl phosphonic acid), abbreviated as phosphonic acid PEG copolymer in the following sections, was synthesized by Specific Polymers, France (http://www.specificpolymers.fr/). The synthesis was carried out by free-radical polymerization from PEG-methacrylate (PEGMA, SP-43-3-002, CAS: 26915-72-0) and dimethyl(methacryoyloxy)-methyl phosphonate (MAPC1, SP-41-003, CAS: 86242-61-7) monomers, leading to the formation of the poly(PEGMA-*co*-MAPC1) statistical polymer (Figure S1). The conversion rates of the PEGMA and MAPC1 monomers were determined during from synthesis and showed similar time dependences, indicating that the copolymers have the same number of PEGs and phosphonic acid groups (Figure S2). For this synthesis, the molecular weights of the PEG pending side chains were 1000, 2000, and 5000 g mol^{-1}, referred to as PEG_{1K}, PEG_{2K}, and PEG_{5K} in the sequel of the article (Figure 1a). Poly(poly(ethylene glycol) methacrylate-*co*-methacrylic acid), in short poly-(PEGMA-*co*-MAA), was synthesized by free-radical polymerization from PEGMA and methacrylic acid (MAA) (CAS: 79-41-4, Acros Organics) monomers (Figure S2). The resulting statistical copolymer is abbreviated as carboxylic acid PEG copolymer. For this synthesis, the molecular weight of the PEG pending side chains studied is 2000 g mol^{-1}.

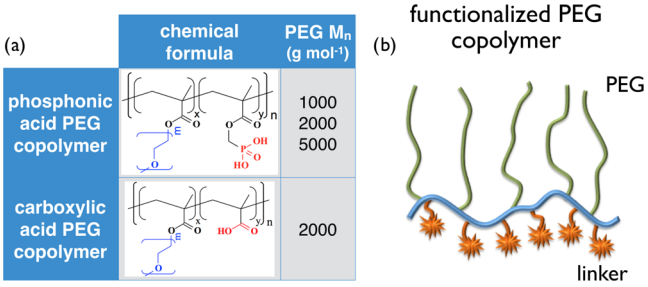

Figure 1. (a) Chemical formulae of the statistical copolymers used in this work. Four copolymers were investigated, three with phosphonic acid and 1000, 2000, and 5000 g mol^{-1} PEG side chains, respectively, and one with carboxylic acid and 2000 g mol^{-1} PEG. (b) Schematic representation of the statistical copolymers.

II.I.II. Characterization by Light Scattering. The weight-averaged molecular weights of the polymers were determined by static light scattering measurements (NanoZS Zetasizer, Malvern). Toluene was used for calibration. The polymer solutions were prepared with 18.2 MΩ MilliQ water and filtered with 0.2 μm cellulose filters, and their pHs were adjusted to 8 by the addition of sodium hydroxide. The scattering intensity was found to vary linearly with concentration between 0 and 1 wt % (Figure S2). The refractive index increment of the different polymer solutions was obtained by refractometry (Arago, Cordouan Technologies), and it was used to calculate the

DOI: 10.1021/acsomega.7b00007
ACS Omega 2017, 2, 1309−1320

polymer scattering contrast. The molecular weights were derived from the Zimm representation and the zero-concentration extrapolated scattering, as detailed in refs 21 and 32. The weight-averaged molecular weights of the four polymers studied are provided in Table 1. They are in good agreement with those of the targeted ones.

Table 1. Structural Parameters of the Phosphonic and Carboxylic PEG Copolymers Used in This Work[a]

terminus	M_n(PEG), g mol^{-1}	M_n, g mol^{-1}	M_w, g mol^{-1}	acid group, meq g^{-1}	funct. group per chain
phosphonic acid	1000	5300	9500	1.58	4.2
	2000	7200	12 950	0.87	3.1
	5000	42 600	76 650	0.35	7.4
carboxylic acid	2000	8600	15 500	0.46	4.0

[a] M_n(PEG) denotes the PEG molecular weight of the pendant side chains and M_n and M_w denote the number and mass averaged molecular weights of the statistical copolymers, respectively, as determined by light scattering. The molar equivalent of acid groups per gram (meq g^{-1}) of polymer was determined from ^{1}H and ^{31}P NMR, leading to estimates of the number of functionalized groups per chain.

For the characterization of the iron oxide particles, dynamic light scattering was performed using NanoZS, at a wavelength of 633 nm and in a close-to-backscattering configuration, that is, with a scattering angle of 173°. From the time dependence of the scattered intensity, the second-order autocorrelation function of the light was calculated and analyzed using the cumulant method and the CONTIN algorithm. Both procedures gave consistent values for the hydrodynamic diameter, D_H. For bare nanoparticles, the hydrodynamic diameters were found to be larger than those obtained by transmission electron microscopy (TEM), attributed to the particle size distribution and the fact that the scattered intensity varies as the sixth power of the particle diameter.

II.I.III. Acid−Base Titration. To study the role of acid functionality in grafting, poly(PEGMA-*co*-MAPC1) and poly(PEGMA-*co*-MAA) adsorptions were performed at two pH values, 2.0 and 7.4. pH 2.0 corresponds to the conditions for coating iron oxide nanoparticles.[21,24,46] Acid−base titration curves have shown the presence of two pK_A's (pK_{A1} = 2.7 and pK_{A2} = 7.8) for the phosphonic acid (Figure S3). For the carboxylic acid, the pK_A was found at 5.5. For the iron oxides, the point of zero charge is observed around pH 8.0. The surface below is positively charged due to the presence of Fe−OH_2^+ groups, whereas the surface above bears negatively charged Fe−O^-.[47,48] It should be mentioned here that the iron oxide nanoparticles tested are made from maghemite γ-Fe_2O_3, whereas the flat substrate is magnetite, Fe_3O_4. As shown by Jolsterå et al. using high-precision potentiometric titrations,[49] the acid/base properties of magnetite are similar to those of maghemite, except for the difference in surface site density, estimated to be 1.50 nm^{-2} for magnetite and 0.99 nm^{-2} for maghemite. For this reason, we assume that the two iron oxide substrates behave similarly with respect to the acidic residues.

II.I.IV. Characterization by Size-Exclusion Chromatography. The molar-mass dispersity, $Đ$, for poly(PEGMA-*co*-MAPC1) and poly(PEGMA-*co*-MAA) was determined by size-exclusion chromatography on a PolyPore column, using tetrahydrofuran as the eluant and polystyrene standards. For PEG_{2K} side chains, molar-mass dispersity $Đ$ was found to be 1.81 and 1.78, respectively.[21]

II.I.V. Characterization by NMR. Phosphonic acid PEG copolymers were characterized by ^{1}H NMR and ^{31}P NMR using a Bruker Avance 300 spectrometer operating at 300 MHz (Figure S4). From the molar equivalent of acid groups per gram obtained by NMR, the average numbers of functional moieties and PEG side chains per chain were derived. They were found to be between 3 and 7, depending on the PEG side chain molecular weight (Table 1). These findings confirm the existence of multiple functional groups on the same polymer backbone (Figure 1b).

II.I.VI. Iron Oxide Nanoparticles. Iron oxide nanocrystals of 6.8 nm diameter were synthesized by co-precipitation of iron(II) and iron(III) salts in aqueous media and by further oxidation of the magnetite (Fe_3O_4) into maghemite (γ-Fe_2O_3).[46,50,51] The as-prepared particles are positively charged and have nitrate counterions on their surfaces. The resulting interparticle interactions are repulsive and provide excellent long-term colloidal stability to the dispersion. The particle size distribution was determined from dynamic light scattering and transmission electron microscopy. The crystalline cubic structure of the particles was assessed by electron beam microdiffraction (Figure S5).[52]

II.I.VII. Nanoparticle Coating. For nanoparticle coating, we used a protocol established in 2008[32,46] and later applied for the development of magnetic resonance imaging contrast agents for in vivo experimentations.[24] Dispersions of particles and PEGylated copolymers were prepared under the same conditions of pH (pH 2.0) and concentration and then mixed at different volume ratios, X. The choice of pH was dictated by the fact that uncoated iron oxide particles aggregate under neutral or alkaline conditions. Following the mixing, the polymers adsorb spontaneously on the particle surfaces due to the acid groups complexing the iron hydroxide sites on the magnetite surface,[32] resulting in an increase in the particle hydrodynamic diameter (Figure 2a). For the PEGylated copolymers studied here, no precipitation or particle aggregation was observed following the mixing at this pH. The pH of the mixed solution was then raised to 8.0 by sodium hydroxide addition, leading to two distinct behaviors. Below a critical mixing ratio, X_C, well-dispersed coated particles were obtained, again, with a D_H slightly larger than that of bare particles. Above X_C, particles precipitate and form large clumps in solution, which eventually sediment. Detailed investigations on polymer coverage as a function of the mixing ratio are discussed in refs 21 and 24.

II.I.VIII. Serum Proteins. Phosphate buffer solution (PBS) was prepared by dissolving one tablet (Sigma-Aldrich) in 200 mL of DI water (Millipore, 18.2 MΩ resistivity). FBS from Gibco Invitrogen, with a nominal composition of 23.9 g L^{-1} BSA, 13.2 g mL^{-1} α-globulin, 4.5 g L^{-1} β-globulin, and 0.155 g L^{-1} γ-globulin was used. The FBS was diluted with PBS at a concentration of 10 vol % and used without further modification.

II.I.IX. Nanoparticle Stability in Physiological and Culture Media. For the evaluation of the particle stability, the following protocol was applied.[46,53] A few microliters of the concentrated dispersion was poured and homogenized rapidly in 1 mL of the solvent to be studied, and simultaneously, the scattered intensity, I_S, and diameter, D_H, were measured by light scattering. After mixing, the measurements were monitored over a 2 h period, and subsequent measurements were made after 24 h and 1 week. The nanoparticles are considered to be stable if their hydrodynamic diameter, D_H, in a given solvent remains constant as a function of

DOI: 10.1021/acsomega.7b00007
ACS Omega 2017, 2, 1309−1320

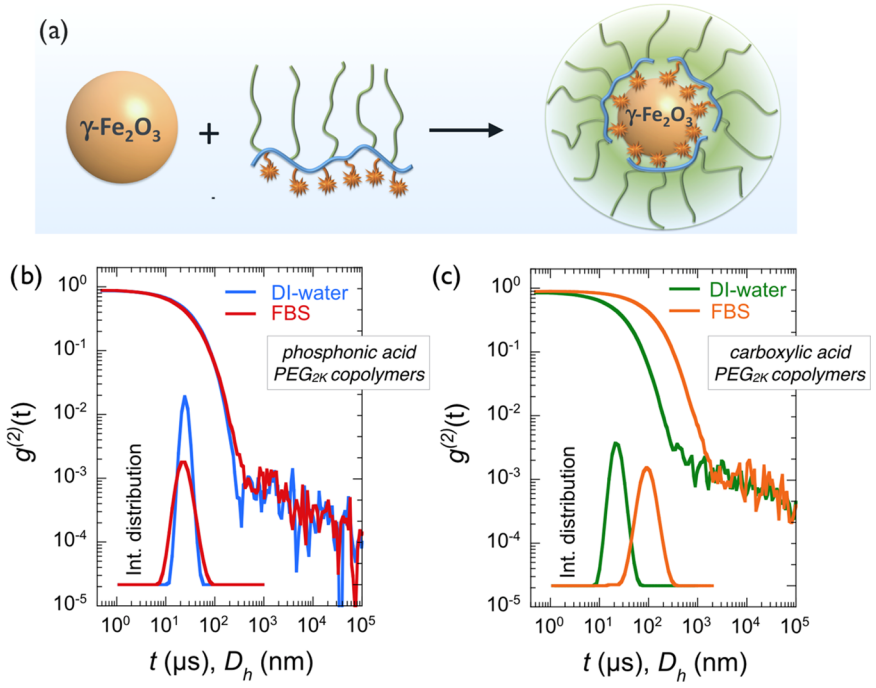

Figure 2. (a) Schematic representation of an iron oxide particle, a multiphosphonic or carboxylic acid PEG copolymer, and the resulting nanostructure made from the two species. (b) Autocorrelation function $g^{(2)}(t)$ of the scattered light obtained from iron oxide nanoparticles coated with phosphonic acid PEG_{2K} copolymers in deionized (DI) water and in fetal bovine serum (FBS)-containing medium. Inset: intensity distribution corresponding to the correlograms. (c) Same as that in (b) for carboxylic acid PEG_{2K} copolymer coating. The data show destabilization of the dispersion and particle agglomeration.

time and equal to its initial value. The solvents surveyed here are DI water (pH 7.4), phosphate buffer saline, and cell culture medium (Dulbecco's modified Eagle's medium) with or without FBS. Stability assays were performed on bare and coated 6.8 nm iron oxide nanoparticles. Examples of temporal behaviors in physiological and cell culture media together with the particle stability diagram are shown in Figure S6.

II.II. QCM. A QCM-D-monitoring equipment (Q-Sense E1 system, Biolin Scientific, Sweden) was used to follow the adsorption kinetics of phosphonic acid and carboxylic acid PEG copolymers on an iron oxide substrate. AT-cut quartz crystal sensors coated with a thin film of magnetite (Fe_3O_4) (Biolin Scientific, Sweden), with a fundamental resonance frequency of 4.95 MHz, were cleaned by 10 min of sonication and exposed to an ultraviolet (UV)/ozone cleaner for 10 min. QCM-D experiments were carried out at 25 ± 0.02 °C in an exchange mode at a flow rate of 100 μL min^{-1}. The injected polymer solutions were prepared at a concentration of 0.1 wt % and pHs of 2.0 and 7.4, adjusted with the addition of sodium hydroxide or hydrochloric acid. At least 0.5 mL of the sample solution was delivered into the chamber containing the crystal sensor (of internal volume 40 μL) to ensure complete liquid exchange. In a typical experiment, the crystal was excited at its fundamental resonance frequency (f_0) through a driving voltage applied across the gold electrodes. Any material adsorbing or desorbing onto the crystal surface induces a decrease or increase in the resonance frequency, $\Delta f_n = f_n - f_0$, of the nth overtone. Δf_n is related to the adsorbed mass per unit area (ng cm^{-2}) through the Sauerbrey equation

$$\Delta m = -C\Delta f_n/n \quad (1)$$

where C is the Sauerbrey constant (17.7 ng s cm^{-2} for a 5 MHz quartz sensor) and n (1, 3, 5, 7, 9, 11, or 13) is the overtone number. An indication of frictional losses due to the viscoelastic properties of the adsorbed layer is provided by changes in dissipation, $\Delta D_n = E_D(n)/2\pi E_S(n)$, where $E_D(n)$ is the energy stored in the sensor crystal and $E_S(n)$ is the energy dissipated by the viscous nature of the surrounding medium for the nth overtone.[54,55] The combination of dissipation measurement and frequency monitoring allows the determination of the adsorbed mass as well as the layer viscoelastic properties.[56] The Sauerbrey equation mentioned previously assumed that the adsorbed film is laterally homogeneous, evenly distributed, and thin and that the change in resonance frequency is solely due to the adsorbed mass, including water hydrodynamically trapped in the film. However, polymer films are soft, that is, they may exhibit viscoelasticity, and therefore the Voigt model is more appropriate for data treatment. The Voigt model uses frequency and dissipation data from multiple overtones to calculate the thickness, shear elastic modulus, and shear viscosity of the adsorbed film.[57−59] In addition, the model assumes that (i) the bulk solution above the layer is purely viscous and Newtonian, (ii) the film is uniform, (iii) the viscoelastic properties of the layer are frequency-independent in the range 5−65 MHz, and (iv) there is no slip between the adsorbed layer and crystal during shearing.[57] In this work, results at overtones (n) 3, 5, 7, 9, 11, and 13 were adjusted to the Voigt model using the QTools software (Biolin Scientific AB, Sweden). The measurements were performed after mounting the crystals in the flow module and establishing a baseline with water. The water was exchanged with PEGylated polymer solution pumped into the chamber. The adsorption behavior of different PEG copolymers at various concentrations on Fe_3O_4 was checked one after another, and DI water at pH 7.4 was used to rinse the layer surface between each deposition step. The adsorption behavior of 10 vol % FBS on the PEG brush was also studied using the same procedure.

DOI: 10.1021/acsomega.7b00007
ACS Omega 2017, 2, 1309−1320

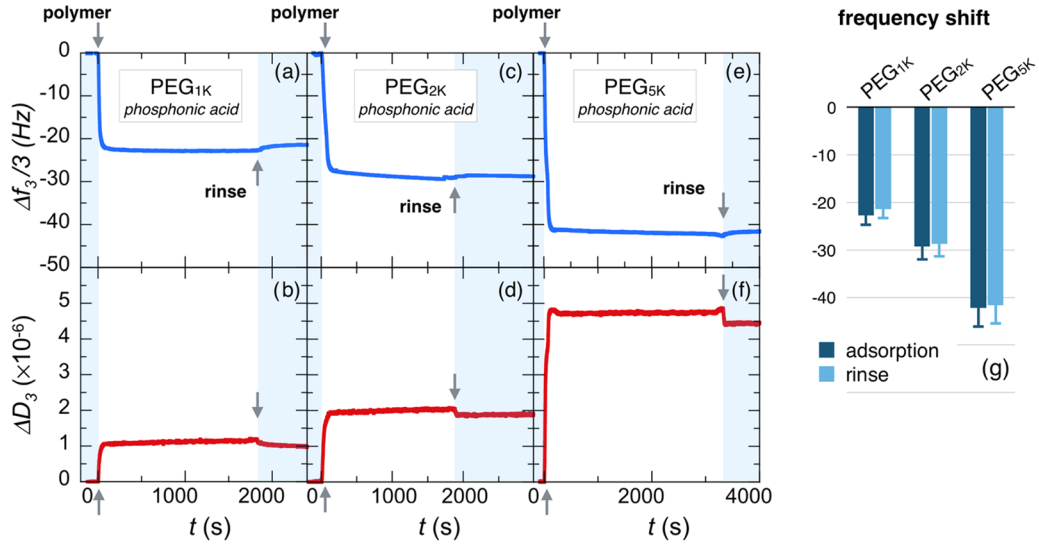

Figure 3. Real-time binding curves for frequency $\Delta f_3/3$ and dissipation ΔD_3 during the adsorption of phosphonic acid PEG copolymers onto Fe_3O_4 substrates at pH 2.0. PEG pending side chains have molecular weights of 1000 g mol^{-1} (a, b), 2000 g mol^{-1} (c, d), and 5000 g mol^{-1} (e, f). The data are those from the third overtone of the QCM-D acoustic device. In each panel, the first arrow at t = 0 denotes the time at which the polymer solution (concentration 0.1 wt %) is injected. The second arrow denotes the time at which DI water (pH 7.4) is introduced for rinsing. (g) Histogram for the steady-state frequencies upon polymer adsorption and rinsing.

III. RESULTS AND DISCUSSION

III.I. Stealth Phosphonic Acid PEG-Coated Nanoparticles. In this work, 6.8 nm iron oxide nanocrystals were coated with phosphonic acid and carboxylic acid PEG copolymers using the formulation pathway described in the Experimental Section.[50−52] In brief, dispersions of the particles and PEGylated copolymers were prepared under the same conditions of pH (pH 2.0) and concentration (c = 0.2 wt %) and mixed at different volume ratios, X. The pH of the mixed solution was raised to 8.0 by sodium hydroxide addition. It was found that below the critical mixing ratio, X_C, equal to 1.5 for both polymers here, well-dispersed coated particles were obtained, with a D_H about 5 nm larger than that of bare particles (Figure 2a). In contrast, above X_C, particles form large aggregates and precipitate in solution (as uncoated particles do), indicating an incomplete surface coverage by the polymers. The dispersions studied here were prepared at X = 0.2, that is, with a large excess of polymers, to ensure that all positive surface charges were complexed by acid groups. The dispersions were then dialyzed against DI water to remove the excess polymers (cutoff membrane 50 and 100 kD). Dynamic light scattering was used to measure the thickness of the polymer layer. For dispersions that are not stable, light scattering also allows estimation of the aggregation kinetics.[46,53] Figure 2b,c displays the second autocorrelation function of the scattered intensity, $g^{(2)}(t)$, for iron oxide coated with phosphonic and carboxylic acid PEG_{2K} copolymers in DI water, respectively. The data exhibit a quasiexponential decay associated with a unique relaxation mode. Derived from the second cumulant coefficient (Z_{ave}), the hydrodynamic diameters were 23.8 and 21.8 nm, with dispersity indexes of 0.08 and 0.18, respectively. These D_H values are 9.8 and 7.8 nm larger than those of the bare particles (D_H = 14 nm[24]) and were ascribed to the layer thickness noted, h_{NP}, to distinguish it from the polymer layer thickness on the flat substrate, h_{2D}, defined in the next section. Here, we found that h_{NP} = 4.5 ± 0.5 nm. With zeta potentials of −2 to −6 mV, electrokinetic measurements confirmed that the PEGylated particles are globally neutral. For PEG_{5K}, the polymer thickness was also determined and found to be 8 ± 1 nm. The values for h_{NP} are consistent with those for stretched PEG chains forming a polymer brush.[38,60] As shown in the insets, the associated intensity distributions are characterized by a single particle size. When dispersed in 10 vol % FBS, the autocorrelation function and intensity distribution remain unchanged for particles with phosphonic acid (D_H = 21.8 nm, pdi = 0.21). This result ascertains that PEGylated particles are stable in a serum rich medium and devoid of protein corona. A comprehensive characterization study has also shown that this stability is being maintained in cell culture media without serum and for an extended period of time (>weeks).[21,24] For particles coated with carboxylic acid-functionalized polymers, the $g^{(2)}(t)$ relaxation is shifted to longer decay times and the intensity distribution is now peaked at D_H = 85.3 nm (pdi = 0.21), indicating a modification of the particle structure. The size increase could be due to protein adsorption on the PEG layer, a scenario that would be compliant with the corona model[3,31,53] or particle aggregation induced by PEG-layer depletion. From the light scattering measurements, it is concluded that the phosphonic acid PEG copolymer is an efficient coating agent compared with its carboxylic acid counterpart. Although the impact of polymer type on particle stability is clear, the nature of the interactions of plasma proteins with a PEG coating layer remains open to question. To answer this question, a series of QCM-D experiments were performed using iron oxide substrates grafted with PEG copolymers.

III.II. Polymer Adsorption on an Fe_3O_4 Substrate. *III.II.I. Effect of PEG Molecular Weight.* Figure 3a,b displays the adsorption profiles obtained by means of the QCM-D technique for the third overtone frequency, $\Delta f_3/3$, and the related dissipation, ΔD_3, of a 0.1 wt % solution of phosphonic acid PEG_{1K} copolymers at pH 2.0 and room temperature, as those for nanoparticle coating.[24] Indeed, at this pH Fe_3O_4 is positively charged, with an estimated density of active $Fe-OH_2^+$ sites of about 1.50 nm^{-2}.[47,49] Upon solution injection (arrow at t = 0), the frequency exhibits a rapid decrease and then a fast saturation at $\Delta f_3/3$ = −22.7 Hz. Similarly, ΔD_3 increases rapidly and reaches a plateau at 1.1 × 10^{6}. On increasing PEG molecular weights as in Figure 3c,d for PEG_{2K} and in Figure 3e,f for PEG_{5K},

DOI: 10.1021/acsomega.7b00007
ACS Omega 2017, 2, 1309−1320

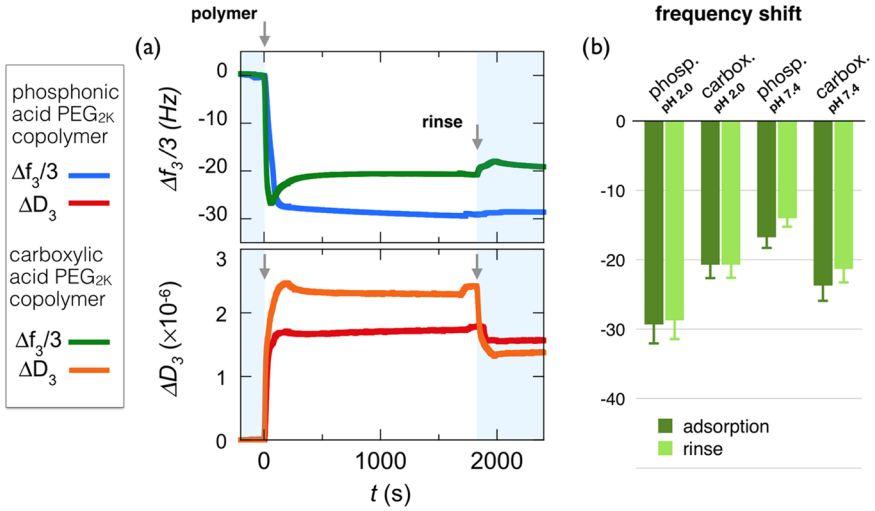

Figure 4. (a) Binding curves for frequency $\Delta f_3/3$ and dissipation ΔD_3 during adsorption of phosphonic acid and carboxylic PEG copolymers on Fe_3O_4 substrates at pH 2.0. PEG side chains are 2000 g mol^{-1} for both copolymers. In each panel, the first arrow at $t = 0$ denotes the time at which the polymer solution (concentration 0.1 wt %) is injected. The second arrow denotes the time at which DI water (pH 7.4) is introduced for rinsing. (b) Histogram for the steady-state frequencies upon polymer adsorption and rinsing at the two pH values, 2.0 and 7.4.

the time-dependent profiles remain basically the same but the $\Delta f_3/3$ decreases to −29.4 Hz (with dissipation $\Delta D_3 = 2.0 \times 10^{-6}$) and −43.3 Hz for PEG_{2K} and −43.3 Hz (with $\Delta D_3 = 4.8 \times 10^{-6}$) for PEG_{5K}. These adsorption kinetics are consistent with that reported by QCM-D upon deposition of polymers on various substrates.[8,41,42,61−64] The polymer-binding curves corresponding to the different overtones (n = 3, 5, 7, 9, and 11) are provided in Figure S7. Figure 3g summarizes the frequency shift data, that is, the adsorbed mass (including the solvation water) for the three molecular weights, indicating that increasing masses are bound to the substrate depending on chain length.[65] After the deposition, rinsing with DI water at pH 7.4 has a little effect on the adsorbed layer for the considered polymers. The relative frequency gains after rinsing are 5%, 2% and 1.4% for PEG_{1K}, PEG_{2K}, and PEG_{5K}, respectively, indicating that the polymer layers are firmly attached to the substrate and that the stability is enhanced for longer chains.

III.II.II. Effect of Acid Groups. The study of layer formation of PEG layers with phosphonic acid and carboxylic acid, respectively, as linkers, at pH 2.0, sheds light on the role of acidic groups of different strengths in the adsorption process. At this acidic pH, indeed phosphonic acid groups are negatively charged, carboxylic acid groups are uncharged, and the Fe_3O_4 substrate is positively charged.[47−49] Figure 4a compares the frequency and dissipation binding curves obtained for PEG_{2K} copolymers functionalized with phosphonic acid and carboxylic acid moieties at pH 2.0 and 25 °C. It can be seen that the carboxylic acid PEG copolymer undergoes a strikingly different adsorption process compared with its phosphonic acid counterpart. In particular, a well-defined undershoot behavior is observed and suggests a fast adsorption/desorption processes due to conformational rearrangement of the adsorbent on oversaturated surfaces.[66,67] Furthermore, the adsorbed mass at saturation is 30% lower than that for phosphonic acid ($\Delta f_3/3$ = −20.6 vs −29.4 Hz), whereas the related dissipation is slightly higher, globally indicating that the less carboxylic acid PEG copolymers are more loosely bound to the Fe_3O_4 substrate than are the phosphonic acid-functionalized chains. Accordingly, upon rinsing, the carboxylic acid-containing polymer shows a slight decrease and an apparent compaction of the bound mass, which are not observed with phosphonic acid.

To further assess the role of the charges on adsorption, experiments were performed at pH 7.4, that is, under conditions in which the phosphonic and carboxylic acid are both negatively charged and the Fe_3O_4 substrate is neutral.[48,49] The degrees of ionization estimated from pK_a's values are 1.3 (indicating that 30% of the phosphonic acid groups bear two negative charges) and 0.8, respectively. Figure 4b summarizes the frequency shifts for the two acid-functionalized PEGs at the two pHs (see Figure S8 for complete adsorption profiles). In particular, the phosphonic acid PEG copolymer suffers a drastic reduction (of about 50%) in the adsorbed mass from pHs 2.0 to 7.4, whereas the carboxylic acid-functionalized PEG mass is adsorbed in comparable amounts at both pHs. Again, rinsing has a negligible effect on the adsorbed masses. Data from Figure 4b suggest that for phosphonic acid-containing polymers, electrostatics is an important driving force for binding to the iron oxide surface, as adsorption is related to opposite-charge pairing and complexation.[41,63] The lower adsorption levels exhibited by carboxylic acid-functionalized PEG may result from the fact that the acid groups and substrate are only weakly charged. In this later case, other binding mechanisms, including H-bonding, might be relevant.[10,68,69] Overall, the data indicate that the most efficient coating and binding to the Fe_3O_4 substrate occurred under acidic conditions, with phosphonic acid groups interacting with protonated Fe−OH_2^+ groups. The two different acidic groups then interact with a strikingly different efficiency, depending on the relative pK_a's of phosphonic and carboxylic acid residues.

III.III. Polymer Brush Structure. Figure 5a shows the relationship between the variation of the dissipation, ΔD_3, and resonance frequency shift, $-\Delta f_3/3$, during the adsorption process of phosphonic acid PEG_{1K}, PEG_{2K}, and PEG_{5K} and carboxylic acid PEG_{2K} at pH 2.0. Previous studies have shown that the slope of the D−f plot reflects the layer viscoelasticity, depending upon processes such as conformational changes, compaction, or hydration/dehydration of the macromolecules at the surface.[55,62] For phosphonic acid-containing polymers, the ratio $-\Delta D_3/(\Delta f_3/3)$ is found to be in the range of $(0.6−1.7) \times 10^{-7}$ Hz^{-1} and remains below the Sauerbrey limit, 4×10^{-7} Hz^{-1},

DOI: 10.1021/acsomega.7b00007
ACS Omega 2017, 2, 1309−1320

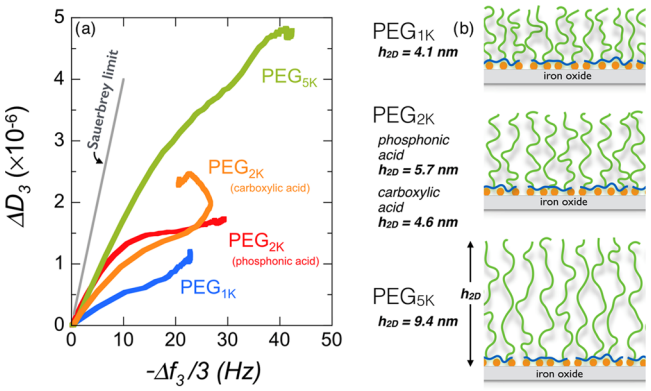

Figure 5. (a) Plot of dissipation, ΔD_3, as a function of the frequency shift, $-\Delta f_3/3$, during the adsorption process of phosphonic acid PEG_{1K}, PEG_{2K}, and PEG_{5K} and carboxylic acid PEG_{2K} at pH 2.0. The straight line represents the Sauerbrey limit (slope 4×10^{-7} Hz^{-1}) valid for homogeneous and rigid films.[54,55] (b) Schematic representation of PEGylated layers deposited on iron oxide substrates obtained for the four polymers in (a). The values of brush thicknesses estimated from the Voigt viscoelastic model are also indicated.[54]

typical of homogeneous and rigid films.[54,55] For the carboxylic acid copolymer PEG_{2K}, the undershoot observed in Figure 4a translates into a change in regime with a negative slope 5 min after injection. The Sauerbrey equation (eq 1) is thus used to derive the areal mass density of the film, which under the present conditions includes both the polymer adsorbate and solvent. With increasing molecular weight, from PEG_{1K} to PEG_{5K}, the areal mass density increases from 400 to 750 ng cm^{-2} for the deposition step at pH 2.0 (Table 2 and Figure S9) and 380 to 740

Table 2. Summary of PEG Copolymers Used in QCM-D Testing at pH 2.0 and of the Parameters Describing Their Brush Properties[a]

terminus	M_n (PEG), g mol^{-1}	mass, ng cm^{-2}	thickness h, nm	PEG density σ_{PEG}, nm^{-2}	PEG reduced density Σ
phosphonic acid	1000	400	4.1	1.55	11.7
	2000	520	5.7	0.53	7.4
	5000	750	9.4	0.15	4.6
carboxylic acid	2000	370	4.6	0.28	3.8

[a]The mass (ng cm^{-2}) is calculated from the Sauerbrey equation (eq 1); the layer thickness, via the Voigt viscoelastic model; and the PEG density, σ_{PEG}, from the polymer brush theory.[39] The reduced tethered density, Σ, is obtained from the expression $\pi\sigma_{PEG}R_g^2$, where $R_g = 7.32 \times 10^{-2} M_w^{0.442}$ denotes the PEG gyration radius.[34,70]

ng cm^{-2} for the rinsing step at pH 7.4. Values in the range 200–1000 ng cm^{-2} are usual for polymers adsorbing spontaneously at interfaces either via physisorption or grafting-to mechanisms.[41,42,61−63]

The hydrodynamic film thickness, h_{2D}, was estimated using the Voigt viscoelastic model.[54,55] In the deposition step, the thickness increases to 4.1, 5.7, and 9.4 nm for phosphonic acid-containing PEG_{1K}, PEG_{2K}, and PEG_{5K} polymers, respectively (Figure 5b). The thickness of carboxylic acid-functionalized PEG_{2K} is 4.6 nm. After rinsing with DI water at pH 7.4, the h_{2D}-values are lowered by 3–10%, the reduction being stronger for PEG_{1K}. The values for the PEG_{2K} and PEG_{5K} brushes are in good agreement with those obtained by Nalam et al. using poly(L-lysine)-*graft*-PEG[63] and by Emilsson et al. using thiol-terminated PEGs.[42] Note also that the thickness of the PEG_{2K} and PEG_{5K} films on flat Fe_3O_4 substrates compares well with that of the nanoparticle coating layer (Section III.I). From light scattering, the spherical brush thicknesses were found to be $h_{NP} = 4.5 \pm 0.5$ and 8.0 ± 1.5 nm for PEG_{2K} and PEG_{5K}, respectively, in excellent agreement with $h_{2D} = 5.7$ and 9.4 nm measured in QCM-D. The slight difference between the two determinations may arise from curvature effects.[60]

To estimate the PEG density at the surface, it is assumed that the layer structure obeys the polymer brush theory[38,60] in the moderate- and high-surface density regimes and that the density, σ_{PEG}, and height, h_{2D}, are linked through the relation[39,40]

$$h_{2D} = \left(\frac{\sigma_{PEG}}{3}\right)^{1/3} b^{2/3} aN \qquad (2)$$

where $a = 0.28$ and $b = 0.72$ nm are the chemical monomer and Kuhn lengths for PEG,[29,42] respectively, and N is the degree of polymerization of the chains. The derived PEG densities are 1.55, 0.57 (0.28), and 0.15 nm^{-2} for PEG_{1K}, PEG_{2K}, and PEG_{5K}, the value in parenthesis being that of carboxylic acid-functionalized copolymers. A commonly used parameter for quantitative characterization of polymer brushes is the reduced tethered density, $\Sigma = \pi\sigma_{PEG}R_g^2$, where R_g is the gyration radius of the chain in the bulk phase.[34] For PEG, we adopt recent small-angle neutron scattering results from Le Coeur and co-workers,[70] who found a dependence of the form $R_g(M_w) = 7.32 \times 10^{-2} M_w^{0.442}$. From the QCM-D data collected from the different polymers, Σ is found to be in the range 3.8–11.7 (Table 2), corresponding to grafting densities in the moderate (carboxylic acid PEG_{2K}, phosphonic acid PEG_{5K}, $1 < \Sigma < 5$) and highly stretched regimes (phosphonic acid PEG_{1K} and phosphonic acid PEG_{2K}, $\Sigma > 5$).[39] This criterion to evaluate polymer stretching is similar to that found in parallel studies focusing on the ratio $L/2R_g$, where L is the distance between tethered points ($L = \sigma_{PEG}^{-1/2}$).[30,71] The decrease in σ_{PEG} by a factor 10 between PEG_{1K} and PEG_{5K} (Table 2) is attributed to excluded volume interaction and steric repulsion between chains during deposition. The already adsorbed chains act as barriers to incoming ones, a mechanism that is more effective for longer chains. As a result, the brush stretching and morphology are different: dense and solidlike for PEG_{1K} and soft and viscoelastic for PEG_{5K}.[42] These differences in structure also appear in the different spreadings of the overtones measured during deposition (Figures S7 and S9).[55] The Voigt viscoelastic model also allows estimation of the adsorbed mass from the layer thickness, h_{2D}.[72] Table S1 in the Supporting Information compares the areal mass densities for phosphonic acid PEG copolymers obtained from the Sauerbrey equation (eq 1) and from the Voigt model, showing good agreement between the two determinations.

In conclusion, phosphonic acid PEG copolymers are shown to adsorb spontaneously at Fe_3O_4 interfaces and acidic pH. The copolymer backbone attaches to the surface via multisite binding, and the PEG side chains organize themselves into moderate-density or highly stretched brushes of a few nanometers. The QCM-D results confirm the data obtained in the bulk phase with iron oxide nanoparticles.[21]

III.IV. Protein Resistance on Phosphonated and Carboxylated PEG-Coated Fe_3O_4 Substrates. We turn now to the protein resistance properties of the PEGylated surfaces. To set a reference, we investigated the QCM-D response of uncoated Fe_3O_4 substrates exposed to 10 vol % FBS. As already mentioned, FBS is a part of cell culture medium and

DOI: 10.1021/acsomega.7b00007
ACS Omega 2017, 2, 1309−1320

contains mostly albumin and globulin proteins. Figures 6a,b displays the real-time kinetics of protein adsorption in terms of

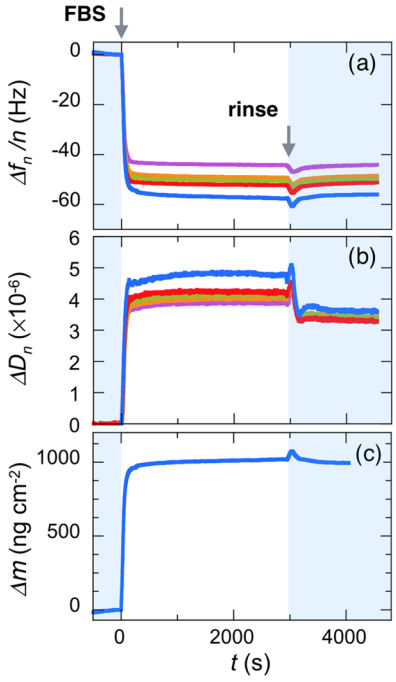

Figure 6. QCM-D responses of uncoated Fe_3O_4 substrates exposed to a 10 vol % FBS solution: (a) harmonic resonance frequency, $\Delta f_n/n$, with n = 3, 5, 7, 9, and 11, (b) corresponding dissipation, ΔD_n, and (c) areal mass density determined from eq 1. The first arrow denotes the FBS injection time and the second arrow, the rinsing time.

frequency shift, $\Delta f_n/n$, and dissipation, ΔD_n, for the different overtones (n = 3−11). After FBS injection, the frequency of the third mode decreases rapidly and levels off at $\Delta f_3/3 = -57.6$ Hz, whereas at the same time, the dissipation increases and reaches $\Delta D_3 = 4.2 \times 10^{-6}$ at steady state. With the ratio $-\Delta D_3/(\Delta f_3/3)$ for proteins being lower than the Sauerbrey limit, the frequency data can be translated into areal mass density, estimated to be 1020 ng cm^{-2} here, at steady state. As for polymer adsorption, the QCM-D data show no change in mass density upon rinsing with DI water at pH 7.4, indicating that proteins are also strongly bound to the Fe_3O_4 surface (Figure 6c). The slight decrease in dissipation is indicative of a deswelling of the protein layer induced by dilution. These findings, together with the values of the protein mass density confirm the strong affinity and resilience of proteins to untreated metal oxide surfaces.[42,56,62]

With PEGylated iron oxide, the adsorption protein behavior changes drastically. In Figure 7a−c, $\Delta f_n/n$ and ΔD_n are plotted for the different overtones following the 10 vol % FBS injection. Stationary frequency shifts for the third mode are $\Delta f_3/3 = -34.2$, −14.3, and −11.5 Hz for PEG_{1K}, PEG_{2K}, and PEG_{5K}, respectively, illustrating that the proteins do adsorb on polymer brushes in various amounts. However, these amounts are lower than those obtained with untreated surfaces. After rinsing, the effect is further amplified. For the PEG_{1K} layer, the residual frequency shift, Δf_{res}, is decreased by a factor 3, whereas for PEG_{2K} and PEG_{5K}, it is reduced to very low frequency shifts, −1.05 and −0.8 Hz, respectively. Related mass densities are 18.6 and 13.6 ng cm^{-2} (Figure 8a), that is, close to the QCM-D detection limit. For these last samples, results suggest that proteins are only loosely attached to the polymer brush and that rinsing at pH 7.4 washes them up. Another crucial result from Figure 7 is that the addition of FBS did not modify the PEG_{2K} and PEG_{5K} layer structures, as both $\Delta f_3/3$ and ΔD_3 returned to their preinjection levels. Figure 8b displays a histogram of the protein areal mass densities deposited on PEGylated substrates obtained under the conditions used in Figure 4b. Here again, phosphonic acid PEG_{2K} polymers show the best results in terms of protein resistance. A schematic representation of the different adsorption

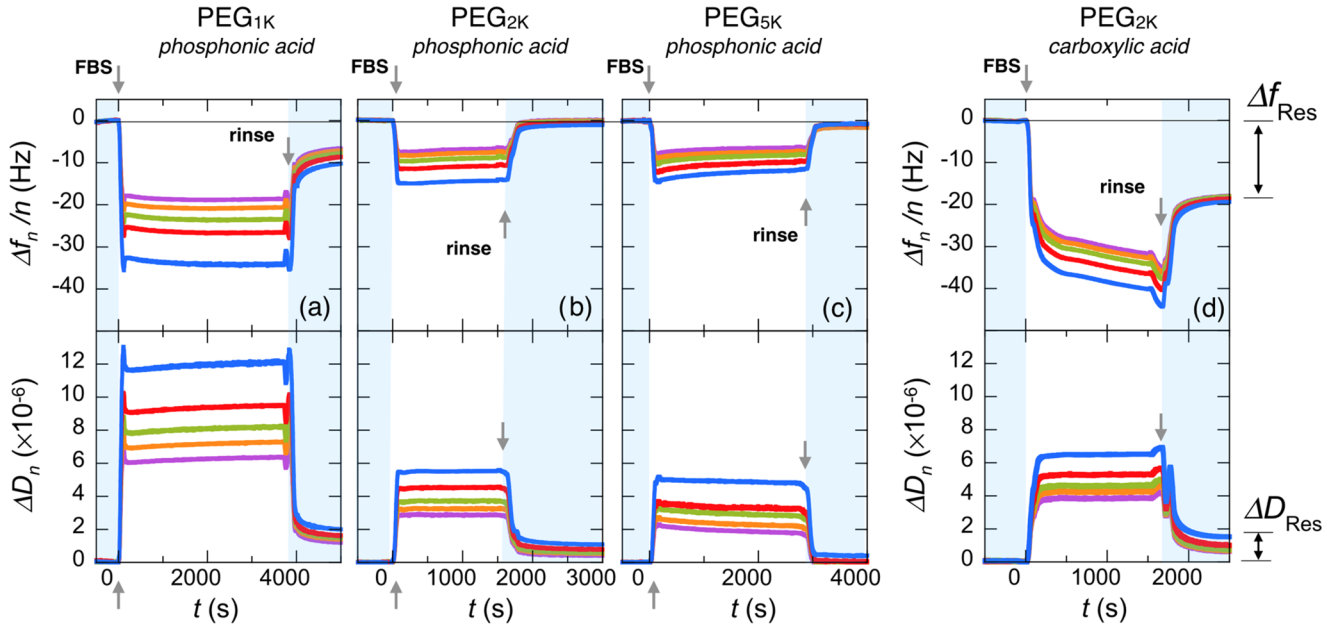

Figure 7. Binding curves for frequency $\Delta f_n/n$ and dissipation ΔD_n (n = 3, 5, 7, 9, and 11) following the injection of a 10 vol % FBS solution. (a−c) Data for phosphonic acid PEG-coated iron oxide with molecular weights of PEG of 1000, 2000, and 5000 g mol^{-1}, respectively. (d) Same as that in (b) for carboxylic acid PEG_{2K} copolymers. For each plot, the first arrow denotes the FBS injection time and the second arrow, the rinsing time. The residual frequency shift and dissipation after rinsing are noted as Δf_{Res} and ΔD_{Res}, respectively.

DOI: 10.1021/acsomega.7b00007
ACS Omega 2017, 2, 1309−1320

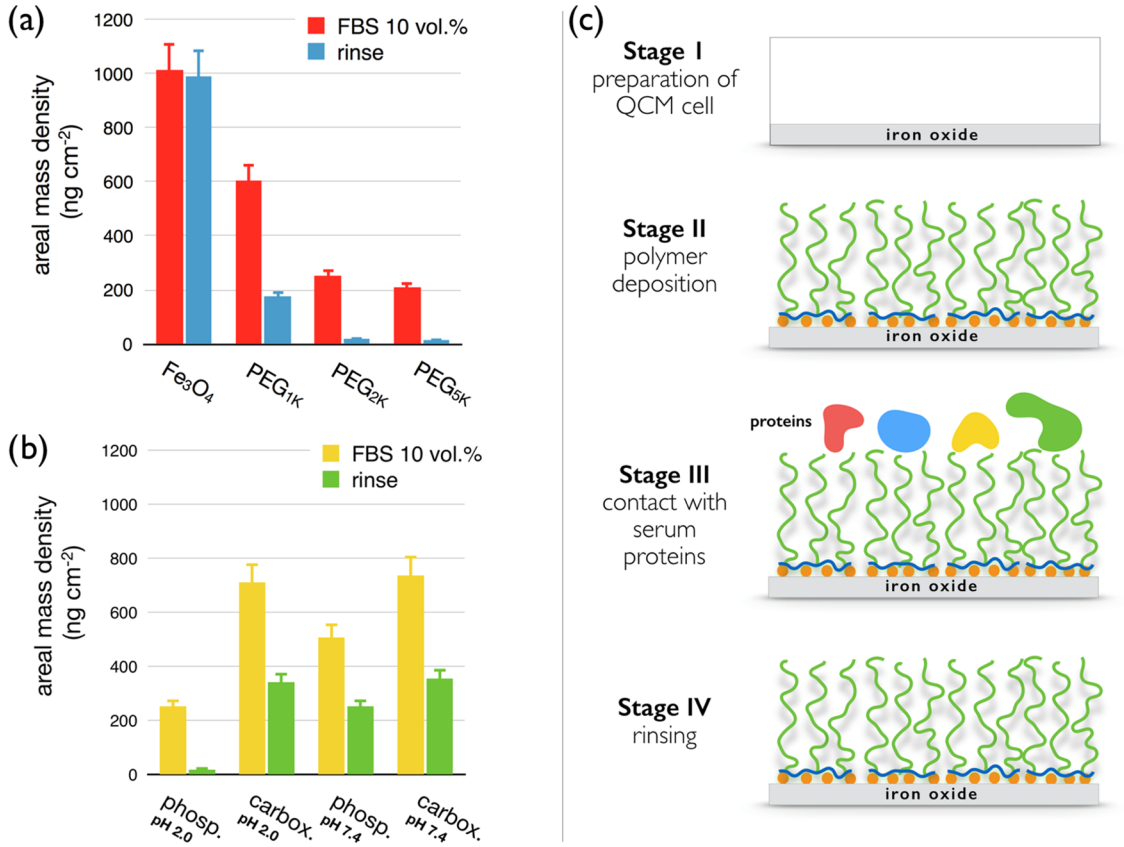

Figure 8. (a) Protein areal mass densities on PEGylated iron oxide substrates for different PEG molecular weights. (b) Same as that in (a) for different brush formation conditions. With a protein resistance of more than 99%, phosphonic acid PEG_{5K} copolymers deposited at pH 2.0 is the most repellent layer. (c) Illustration of the different adsorption and rinsing stages used in the QCM-D protocols, including cell preparation (stage I), polymer deposition (stage II), exposition to serum proteins (stage III), and final rinsing (stage IV).

steps for phosphonic acid-grafted $PEG_{2,5K}$ layers is shown in Figure 8c.

With carboxylic acid PEG copolymers (Figure 7d), the QCM-D response occurs through a rapid decrease in the frequency shortly after injection, followed by a linear drift of the signal. After 30 min, $\Delta f_3/3$ continues to decrease and reaches −40 Hz, that is, three times that found with phosphonic acid-functionalized copolymers. A similar behavior is obtained for ΔD_3, which exhibits no saturation plateau. Rinsing keeps a rather high residual coverage, associated with a frequency shift of −20 Hz and a dissipation of $\Delta D_3 = 2 \times 10^{-6}$. These findings confirm our hypothesis that carboxylic acid-containing polymers are less efficient against protein adsorption. The continuously varying QCM signal following protein injection could indicate a progressive degradation of the PEG layer, due to, for instance, the competitive complexation between the added proteins and grafted copolymers. For all polymers studied, the coverage bioresistance can be evaluated from the residual areal mass densities measured on coated and bare surfaces.[8,30,62] The protein adsorption resistance coefficients for phosphonic acid PEG copolymers are 82, 98, and 99% for PEG_{1K}, PEG_{2K}, and PEG_{5K}, whereas it is only 65% for the carboxylic acid-containing polymers. Polymer adsorption at pH 7.4 does not impart resistant coating, as bioresistance percentages are between 60 and 80%. In conclusion, the most repellent layer is that made from phosphonic acid-functionalized PEG_{5K} deposited at pH 2.0. On the whole, the QCM-D results suggest that the agglomeration of the iron oxide particles coated with carboxylic acid PEG copolymers in 10 vol % FBS (Figure 2b) is due to the combined processes of protein adsorption and brush collapse. This latter phenomenon is also not present with particles coated with phosphonic acid PEG copolymers.

IV. CONCLUSIONS

In this work, we aim to explain recent results on the pharmacokinetics of sub-10 nm iron oxide particles that are able to travel in the blood compartment of mice for more than 2 h without being detected by the mononuclear phagocytic system or cleared by the kidneys or the liver. For in vivo assays, the particles were coated with PEGylated polymers specifically synthesized for biomedical applications and their in vivo distribution was monitored by time-resolved magnetic resonance imaging. It should be recalled here that the same core particles without a PEG coating have circulation lifetimes of a few minutes, that is, typically 50 times shorter than those of the PEGylated ones. At the molecular level, it could be shown that this remarkable property results from the polymer multisite attachment at the particle surface and from the adlayer structure. Here, we re-examine the issue of nanoparticle stability in protein-rich media. For copolymers with identical architectures and differing in their acidic residues, it is demonstrated that the long-term colloidal stability is excellent only with phosphonic acid groups as surface linkers and that in this case the coated particles are devoid of a protein corona. For the particles grafted with carboxylic acid groups, immediate destabilization of the dispersion is observed, suggesting a protein-induced effect toward the coating.

DOI: 10.1021/acsomega.7b00007
ACS Omega 2017, 2, 1309−1320

To test this hypothesis, QCM-D experiments are performed using iron oxide substrates. In a first investigation, the deposition of different copolymers either with phosphonic acid or carboxylic acid is conducted under different pH conditions and PEG molecular weights. Overall, the areal mass density and dissipation coefficient indicate that the most efficient binding to Fe_3O_4 substrates occurs under acidic conditions, with phosphonic residues interacting with protonated $Fe-OH_2^+$ groups. These findings suggest a grafting-to process driven by complexation and pairing of electric charges. Estimated from the Voigt model,[55] the hydrodynamic film thickness of the flat iron oxide substrate is found to be identical to that of the nanoparticles, indicating similar chain conformations in both cases. Comparison with theoretical models allows concluding that the adlayer forms a polymer brush in the moderate or highly stretched regimes. PEG densities (σ_{PEG} = 0.15−1.5 nm^{-2}) and stretching parameters ($\sum$ = 3.8−11.7) are also estimated.

In a second part, the protein resistance of PEGylated built-up substrates is assessed. The main result that emerges from the QCM-D measurement is that whatever the layer extension and grafted PEG density proteins do transiently adsorb onto polymer brushes in various amounts. However, for the PEG_{2K} and PEG_{5K} polymers in combination with phosphonic acid residues rinsing is able to wash the proteins away, leading to substrate protein resistance efficacy close to 100%. More importantly, it is found that in the above two cases the addition of FBS does not modify the layer structure. In contrast, PEG layers prepared at neutral pH, with PEG_{1K} or from copolymers with carboxylic moieties are globally inefficient against protein adsorption. With such coatings, the protein resistance is mitigated down to 60−80%. The present study establishes a clear correlation between the behavior of PEGylated nanoparticles in biological environments and the protein resistance of PEGylated surfaces made from the same building blocks. In conclusion, in the development of novel formulations for nanomedicine, it is essential that the physicochemical properties of the probes be predicted to a high degree of accuracy and the new approaches challenge the paradigm of the protein corona. The present work provides answers to these two major questions, confirming that these goals can be achieved thanks to tunable functional polymers.

■ ASSOCIATED CONTENT

Supporting Information

The Supporting Information is available free of charge on the ACS Publications website at DOI: 10.1021/acsomega.7b00007.

Sections on polymer synthesis (S1) and characterization (S2), acid−base titration of the phosphonic acid-containing polymers (S3), and NMR characterization (S4); TEM data on the iron oxide particles and on the particle stability in biological media, respectively (S5, S6); S7 displays the binding kinetics as a function of the polymer molecular weight for the different overtones, whereas S8 compares the phosphonic and carboxylic acid PEG copolymer adsorptions as a function of pH. the mass kinetic adsorption curve of phosphonic acid PEG copolymers on Fe_3O_4 substrates (S9); S10 compares the QCM-D data analyzed according the Sauerbrey and Voigt models (PDF)

■ AUTHOR INFORMATION

Corresponding Authors

*E-mail: ngiambla@unict.it (N.G.).

*E-mail: gmarletta@unict.it (G.M.).

*E-mail: jean-francois.berret@univ-paris-diderot.fr (J.F.B.).

ORCID

Jean-François Berret: 0000-0001-5458-8653

Notes

The authors declare no competing financial interest.

■ ACKNOWLEDGMENTS

The authors thank Armelle Baeza, Victor Baldim, Nathalie Mignet, Fanny Mousseau, Evdokia Oikonomou, and Chloé Puisney for fruitful discussions. The Laboratoire de PHysico-chimie des Electrolytes et Nanosystèmes InterfaciauX (PHENIX, UMR Université Pierre et Marie Curie-CNRS no. 8234) is acknowledged for providing us with magnetic nanoparticles. Agence Nationale de la Recherche (ANR) and Commissariat à l'Investissement d'Avenir (CGI) are gratefully acknowledged for their financial support of this work through Labex SEAM (Science and Engineering for Advanced Materials and devices) ANR 11 LABX 086, ANR 11 IDEX 05 02. This research was supported in part by the Agence Nationale de la Recherche under the contract ANR-12-CHEX-0011 (PULMONANO). G.M. and N.G. gratefully acknowledge the financial support to this work from the Project FIRB "Accordi di Programma" (MIUR, Rome, Italy), contract no. RBAP11ZJFA_002.

■ REFERENCES

(1) Wilhelm, S.; Tavares, A. J.; Dai, Q.; Ohta, S.; Audet, J.; Dvorak, H. F.; Chan, W. C. W. Analysis of nanoparticle delivery to tumours. *Nat. Rev. Mater.* **2016**, *1*, No. 16014, DOI: 10.1038/natrevmats.2016.14.

(2) Bazile, D.; Prudhomme, C.; Bassoullet, M. T.; Marlard, M.; Spenlehauer, G.; Veillard, M. Stealth me.PEG-PLA nanoparticles avoid uptake by the mononuclear phagocytes system. *J. Pharm. Sci.* **1995**, *84*, 493−498.

(3) Jokerst, J. V.; Lobovkina, T.; Zare, R. N.; Gambhir, S. S. Nanoparticle PEGylation for imaging and therapy. *Nanomedicine* **2011**, *6*, 715−728.

(4) Higaki, Y.; Kobayashi, M.; Murakami, D.; Takahara, A. Anti-fouling behavior of polymer brush immobilized surfaces. *Polym. J.* **2016**, *48*, 325−331.

(5) Jeon, S. I.; Andrade, J. D. Protein—surface interactions in the presence of polyethylene oxide. *J. Colloid Interface Sci.* **1991**, *142*, 159−166.

(6) Jeon, S. I.; Lee, J. H.; Andrade, J. D.; De Gennes, P. G. Protein—surface interactions in the presence of polyethylene oxide. *J. Colloid Interface Sci.* **1991**, *142*, 149−158.

(7) Poncin-Epaillard, F.; Vrlinic, T.; Debarnot, D.; Mozetic, M.; Coudreuse, A.; Legeay, G.; El Moualij, B.; Zorzi, W. Surface treatment of polymeric materials controlling the adhesion of biomolecules. *J. Funct. Biomater.* **2012**, *3*, 528−543.

(8) Chen, H.; Zhao, C.; Zhang, M.; Chen, Q.; Ma, J.; Zheng, J. Molecular understanding and structural-based design of polyacrylamides and polyacrylates as antifouling materials. *Langmuir* **2016**, *32*, 3315−3330.

(9) Hillaireau, H.; Couvreur, P. Nanocarriers' entry into the cell: Relevance to drug delivery. *Cell. Mol. Life Sci.* **2009**, *66*, 2873−2896.

(10) Krishnamoorthy, M.; Hakobyan, S.; Ramstedt, M.; Gautrot, J. E. Surface-initiated polymer brushes in the biomedical field: Applications in membrane science, biosensing, cell culture, regenerative medicine and antibacterial coatings. *Chem. Rev.* **2014**, *114*, 10976−11026.

(11) Monge, S.; Canniccioni, B.; Graillot, A.; Robin, J.-J. Phosphorus-containing polymers: A great opportunity for the biomedical field. *Biomacromolecules* **2011**, *12*, 1973−1982.

(12) Hu, C.-M. J.; Zhang, L.; Aryal, S.; Cheung, C.; Fang, R. H.; Zhang, L. Erythrocyte membrane-camouflaged polymeric nanoparticles as a biomimetic delivery platform. *Proc. Natl. Acad. Sci. U.S.A.* **2011**, *108*, 10980−10985.

DOI: 10.1021/acsomega.7b00007
ACS Omega 2017, 2, 1309−1320

(13) Chapel, J. P.; Berret, J.-F. Versatile electrostatic assembly of nanoparticles and polyelectrolytes: Coating, clustering and layer-by-layer processes. *Curr. Opin. Colloid Interface Sci.* **2012**, *17*, 97−105.
(14) Stuart, M. A. C.; Huck, W. T. S.; Genzer, J.; Mueller, M.; Ober, C.; Stamm, M.; Sukhorukov, G. B.; Szleifer, I.; Tsukruk, V. V.; Urban, M.; Winnik, F.; Zauscher, S.; Luzinov, I.; Minko, S. Emerging applications of stimuli-responsive polymer materials. *Nat. Mater.* **2010**, *9*, 101−113.
(15) Bilek, M. M.; McKenzie, D. R. Plasma modified surfaces for covalent immobilization of functional biomolecules in the absence of chemical linkers: towards better biosensors and a new generation of medical implants. *Biophys. Rev.* **2010**, *2*, 55−65.
(16) Formosa, F.; Sánchez-Vaquero, V.; Rodríguez-Navas, C.; Muñoz-Noval, Á.; Tejera-Sanchez, N.; Silván, M. M.; García-Ruiz, J. P.; Marletta, G. Evaluation of plasma modified polycaprolactone honeycomb scaffolds by human mesenchymal stem cells cultured in vitamin d differentiation medium. *Plasma Processes Polym.* **2010**, *7*, 794−801.
(17) Marletta, G. Ion-Beam Modification of Polymer Surfaces for Biological Applications. In *Materials Science with Ion Beams*; Bernas, H., Ed.; Springer: Berlin, 2010; pp 345−369.
(18) Gillich, T.; Benetti, E. M.; Rakhmatullina, E.; Konradi, R.; Li, W.; Zhang, A.; Schluter, A. D.; Textor, M. Self-assembly of focal point oligo-catechol ethylene glycol dendrons on titanium oxide surfaces: Adsorption kinetics, surface characterization, and nonfouling properties. *J. Am. Chem. Soc.* **2011**, *133*, 10940−10950.
(19) Amstad, E.; Gillich, T.; Bilecka, I.; Textor, M.; Reimhult, E. Ultrastable iron oxide nanoparticle colloidal suspensions using dispersants with catechol-derived anchor groups. *Nano Lett.* **2009**, *9*, 4042−4048.
(20) Basti, H.; Ben Tahar, L.; Smiri, L. S.; Herbst, F.; Vaulay, M. J.; Chau, F.; Ammar, S.; Benderbous, S. Catechol derivatives-coated Fe3O4 and gamma-Fe2O3 nanoparticles as potential MRI contrast agents. *J. Colloid Interface Sci.* **2010**, *341*, 248−254.
(21) Torrisi, V.; Graillot, A.; Vitorazi, L.; Crouzet, Q.; Marletta, G.; Loubat, C.; Berret, J.-F. Preventing corona effects: Multiphosphonic acid poly(ethylene glycol) copolymers for stable stealth iron oxide nanoparticles. *Biomacromolecules* **2014**, *15*, 3171−3179.
(22) Das, M.; Mishra, D.; Dhak, P.; Gupta, S.; Maiti, T. K.; Basak, A.; Pramanik, P. Biofunctionalized, phosphonate-grafted, ultrasmall iron oxide nanoparticles for combined targeted cancer therapy and multimodal imaging. *Small* **2009**, *5*, 2883−2893.
(23) Sandiford, L.; Phinikaridou, A.; Protti, A.; Meszaros, L. K.; Cui, X. J.; Yan, Y.; Frodsham, G.; Williamson, P. A.; Gaddum, N.; Botnar, R. M.; Blower, P. J.; Green, M. A.; de Rosales, R. T. M. Bisphosphonate-anchored PEGylation and radiolabeling of superparamagnetic iron oxide: Long-circulating nanoparticles for in vivo multimodal (T1 MRI-SPECT) imaging. *ACS Nano* **2013**, *7*, 500−512.
(24) Ramniceanu, G.; Doan, B. T.; Vezignol, C.; Graillot, A.; Loubat, C.; Mignet, N.; Berret, J. F. Delayed hepatic uptake of multi-phosphonic acid poly(ethylene glycol) coated iron oxide measured by real-time magnetic resonance imaging. *RSC Adv.* **2016**, *6*, 63788−63800.
(25) Gref, R.; Luck, M.; Quellec, P.; Marchand, M.; Dellacherie, E.; Harnisch, S.; Blunk, T.; Muller, R. H. 'Stealth' corona-core nanoparticles surface modified by polyethylene glycol (PEG): influences of the corona (PEG chain length and surface density) and of the core composition on phagocytic uptake and plasma protein adsorption. *Colloids Surf., B* **2000**, *18*, 301−313.
(26) Inutsuka, M.; Yamada, N. L.; Ito, K.; Yokoyama, H. High density polymer brush spontaneously formed by the segregation of amphiphilic diblock copolymers to the polymer/water interface. *ACS Macro Lett.* **2013**, *2*, 265−268.
(27) Jin, J.; Han, Y. Y.; Zhang, C.; Liu, J. C.; Jiang, W.; Yin, J. H.; Liang, H. J. Effect of grafted PEG chain conformation on albumin and lysozyme adsorption: A combined study using QCM-D and DPI. *Colloids Surf., B* **2015**, *136*, 838−844.
(28) Nagasaki, Y. Construction of a densely poly(ethylene glycol)-chain-tethered surface and its performance. *Polym. J.* **2011**, *43*, 949−958.
(29) Oesterhelt, F.; Rief, M.; Gaub, H. E. Single molecule force spectroscopy by AFM indicates helical structure of poly(ethylene-glycol) in water. *New J. Phys.* **1999**, *1*, No. 6.
(30) Ogaki, R.; Andersen, O. Z.; Jensen, G. V.; Kolind, K.; Kraft, D. C. E.; Pedersen, J. S.; Foss, M. Temperature-induced ultradense peg polyelectrolyte surface grafting provides effective long-term bioresistance against mammalian cells, serum, and whole blood. *Biomacromolecules* **2012**, *13*, 3668−3677.
(31) Pelaz, B.; del Pino, P.; Maffre, P.; Hartmann, R.; Gallego, M.; Rivera-Fernandez, S.; de la Fuente, J. M.; Nienhaus, G. U.; Parak, W. J. Surface functionalization of nanoparticles with polyethylene glycol: Effects on protein adsorption and cellular uptake. *ACS Nano* **2015**, *9*, 6996−7008.
(32) Qi, L.; Sehgal, A.; Castaing, J. C.; Chapel, J. P.; Fresnais, J.; Berret, J.-F.; Cousin, F. Redispersible hybrid nanopowders: Cerium oxide nanoparticle complexes with phosphonated-PEG oligomers. *ACS Nano* **2008**, *2*, 879−888.
(33) Sofia, S. J.; Premnath, V.; Merrill, E. W. Poly(ethylene oxide) grafted to silicon surfaces: Grafting density and protein adsorption. *Macromolecules* **1998**, *31*, 5059−5070.
(34) Cabane, B.; Duplessix, R. Neutron scattering study of water-soluble polymers adsorbed on surfactant micelles. *Colloids Surf.* **1985**, *13*, 19−33.
(35) Leckband, D.; Sheth, S.; Halperin, A. Grafted poly(ethylene oxide) brushes as nonfouling surface coatings. *J. Biomater. Sci., Polym. Ed.* **1999**, *10*, 1125−1147.
(36) Alexander, S. Adsorption of chain molecules with a polar head a scaling description. *J. Phys.* **1977**, *38*, 983−987.
(37) de Gennes, P. G. Conformations of polymers attached to an interface. *Macromolecules* **1980**, *13*, 1069−1075.
(38) Milner, S. T. Polymer brushes. *Science* **1991**, *251*, 905−914.
(39) Brittain, W. J.; Minko, S. A structural definition of polymer brushes. *J. Polym. Sci., Part A: Polym. Chem.* **2007**, *45*, 3505−3512.
(40) Kim, M.; Schmitt, S. K.; Choi, J. W.; Krutty, J. D.; Gopalan, P. From self-assembled monolayers to coatings: Advances in the synthesis and nanobio applications of polymer brushes. *Polymers* **2015**, *7*, 1346−1378.
(41) Delcroix, M. F.; Demoustier-Champagne, S.; Dupont-Gillain, C. C. Quartz crystal microbalance study of ionic strength and pH-dependent polymer conformation and protein adsorption/desorption on paa, peo, and mixed peo/paa brushes. *Langmuir* **2014**, *30*, 268−277.
(42) Emilsson, G.; Schoch, R. L.; Feuz, L.; Höök, F.; Lim, R. Y. H.; Dahlin, A. B. Strongly stretched protein resistant poly(ethylene glycol) brushes prepared by grafting-to. *ACS Appl. Mater. Interfaces* **2015**, *7*, 7505−7515.
(43) Dehghani, E. S.; Spencer, N. D.; Ramakrishna, S. N.; Benetti, E. M. Crosslinking polymer brushes with ethylene glycol-containing segments: Influence on physicochemical and antifouling properties. *Langmuir* **2016**, *32*, 10317−10327.
(44) Graillot, A.; Monge, S.; Faur, C.; Bouyer, D.; Robin, J.-J. Synthesis by RAFT of innovative well-defined (co) polymers from a novel phosphorus-based acrylamide monomer. *Polym. Chem.* **2013**, *4*, 795−803.
(45) Zoulalian, V.; Zurcher, S.; Tosatti, S.; Textor, M.; Monge, S.; Robin, J. J. Self-assembly of poly(ethylene glycol)-poly(alkyl phosphonate) terpolymers on titanium oxide surfaces: Synthesis, interface characterization, investigation of nonfouling properties, and long-term stability. *Langmuir* **2010**, *26*, 74−82.
(46) Chanteau, B.; Fresnais, J.; Berret, J.-F. Electrosteric enhanced stability of functional sub-10 nm cerium and iron oxide particles in cell culture medium. *Langmuir* **2009**, *25*, 9064−9070.
(47) Lucas, I. T.; Durand-Vidal, S.; Dubois, E.; Chevalet, J.; Turq, P. Surface charge density of maghemite nanoparticles: Role of electrostatics in the proton exchange. *J. Phys. Chem. C* **2007**, *111*, 18568−18576.
(48) Schwertmann, U.; Cornell, R. M. *Iron Oxides in the Laboratory: Preparation and Characterization*; Wiley-VCH: Weinheim, 2000.
(49) Jolsterå, R.; Gunneriusson, L.; Holmgren, A. Surface complexation modeling of Fe3O4−H+ and Mg(II) sorption onto maghemite and magnetite. *J. Colloid Interface Sci.* **2012**, *386*, 260−267.

DOI: 10.1021/acsomega.7b00007
ACS Omega 2017, 2, 1309−1320

(50) Berret, J.-F.; Sehgal, A.; Morvan, M.; Sandre, O.; Vacher, A.; Airiau, M. Stable oxide nanoparticle clusters obtained by complexation. *J. Colloid Interface Sci.* **2006**, *303*, 315−318.
(51) Fresnais, J.; Yan, M.; Courtois, J.; Bostelmann, T.; Bee, A.; Berret, J. F. Poly(acrylic acid)-coated iron oxide nanoparticles: Quantitative evaluation of the coating properties and applications for the removal of a pollutant dye. *J. Colloid Interface Sci.* **2013**, *395*, 24−30.
(52) Berret, J.-F.; Sandre, O.; Mauger, A. Size distribution of superparamagnetic particles determined by magnetic sedimentation. *Langmuir* **2007**, *23*, 2993−2999.
(53) Safi, M.; Courtois, J.; Seigneuret, M.; Conjeaud, H.; Berret, J.-F. The effects of aggregation and protein corona on the cellular internalization of iron oxide nanoparticles. *Biomaterials* **2011**, *32*, 9353−9363.
(54) Dixon, M. C. Quartz crystal microbalance with dissipation monitoring: enabling real-time characterization of biological materials and their interactions. *J. Biomol. Tech.* **2008**, *19*, 151−158.
(55) Reviakine, I.; Johannsmann, D.; Richter, R. P. Hearing what you cannot see and visualizing what you hear: Interpreting quartz crystal microbalance data from solvated interfaces. *Anal. Chem.* **2011**, *83*, 8838−8848.
(56) Hemmersam, A. G.; Rechendorff, K.; Foss, M.; Sutherland, D. S.; Besenbacher, F. Fibronectin adsorption on gold, Ti-, and Ta-oxide investigated by QCM-D and RSA modelling. *J. Colloid Interface Sci.* **2008**, *320*, 110−116.
(57) Rodahl, M.; Höök, F.; Fredriksson, C.; Keller, C. A.; Krozer, A.; Brzezinski, P.; Voinova, M.; Kasemo, B. Simultaneous frequency and dissipation factor QCM measurements of biomolecular adsorption and cell adhesion. *Faraday Discuss.* **1997**, *107*, 229−246.
(58) Höök, F.; Kasemo, B.; Nylander, T.; Fant, C.; Sott, K.; Elwing, H. Variations in coupled water, viscoelastic properties, and film thickness of a Mefp-1 protein film during adsorption and cross-linking: A quartz crystal microbalance with dissipation monitoring, ellipsometry, and surface plasmon resonance study. *Anal. Chem.* **2001**, *73*, 5796−5804.
(59) Voinova, M. V.; Rodahl, M.; Jonson, M.; Kasemo, B. Viscoelastic acoustic response of layered polymer films at fluid-solid interfaces: Continuum mechanics approach. *Phys. Scr.* **1999**, *59*, 391.
(60) Daoud, M.; Cotton, J. P. Star shaped polymers - a model for the conformation and its concentration-dependence. *J. Phys.* **1982**, *43*, 531−538.
(61) Delcroix, M. F.; Laurent, S.; Huet, G. L.; Dupont-Gillain, C. C. Protein adsorption can be reversibly switched on and off on mixed PEO/PAA brushes. *Acta Biomater.* **2015**, *11*, 68−79.
(62) Jia, P. X.; He, M.; Gong, Y. K.; Chu, X.; Yang, J. F.; Zhao, J. Probing the adjustments of macromolecules during their surface adsorption. *ACS Appl. Mater. Interfaces* **2015**, *7*, 6422−6429.
(63) Nalam, P. C.; Daikhin, L.; Espinosa-Marzal, R. M.; Clasohm, J.; Urbakh, M.; Spencer, N. D. Two-fluid model for the interpretation of quartz crystal microbalance response: Tuning properties of polymer brushes with solvent mixtures. *J. Phys. Chem. C* **2013**, *117*, 4533−4543.
(64) Schoch, R. L.; Lim, R. Y. H. Non-interacting molecules as innate structural probes in surface plasmon resonance. *Langmuir* **2013**, *29*, 4068−4076.
(65) Fu, L.; Chen, X.; He, J.; Xiong, C.; Ma, H. Study viscoelasticity of ultrathin poly(oligo(ethylene glycol) methacrylate) brushes by a quartz crystal microbalance with dissipation. *Langmuir* **2008**, *24*, 6100−6106.
(66) Ohshima, H.; Sato, H.; Matsubara, H.; Hyono, A.; Okubo, M. A theory of adsorption kinetics with time delay and its application to overshoot and oscillation in the surface tension of gelatin solution. *Colloid Polym. Sci.* **2004**, *282*, 1174−1178.
(67) Filippov, L. K.; Filippova, N. L. Overshoots of adsorption kinetics. *J. Colloid Interface Sci.* **1996**, *178*, 571−580.
(68) Srinivasan, N.; Bhagawati, M.; Ananthanarayanan, B.; Kumar, S. Stimuli-sensitive intrinsically disordered protein brushes. *Nat. Commun.* **2014**, *5*, No. 5145.
(69) Furusawa, H.; Sekine, T.; Ozeki, T. Hydration and viscoelastic properties of high- and low-density polymer brushes using a quartz-crystal microbalance based on admittance analysis (qcm-a). *Macromolecules* **2016**, *49*, 3463−3470.
(70) Le Coeur, C.; Teixeira, J.; Busch, P.; Longeville, S. Compression of random coils due to macromolecular crowding: Scaling effects. *Phys. Rev. E: Stat., Nonlinear, Soft Matter Phys.* **2010**, *81*, No. 061914.
(71) Perry, S. S.; Yan, X. P.; Limpoco, F. T.; Lee, S.; Muller, M.; Spencer, N. D. Tribological properties of poly(l-lysine)-graft-poly-(ethylene glycol) films: Influence of polymer architecture and adsorbed conformation. *ACS Appl. Mater. Interfaces* **2009**, *1*, 1224−1230.
(72) Fang, J. J.; Ren, C. L.; Zhu, T.; Wang, K. Y.; Jiang, Z. Y.; Ma, Y. Q. A. Comparison of the different responses of surface plasmon resonance and quartz crystal microbalance techniques at solid-liquid interfaces under various experimental conditions. *Analyst* **2015**, *140*, 1323−1336.

DOI: 10.1021/acsomega.7b00007
ACS Omega 2017, 2, 1309−1320